High-resolution Radiation Characterization for an Uniformly Emitted SiNx Nanophotonic Phased Array

Caiming Sun[1,2], Binghui Li[1], Ning Ding[1], and Aidong Zhang[1,*]
[1]*Shenzhen Institute of Artificial Intelligence and Robotics for Society (AIRS), The Chinese University of Hong Kong (CUHK), Shenzhen, China*
[2]*Peng Cheng Laboratory (PCL), Shenzhen 518055, Guangdong, China*
Author e-mail address: zhangaidong@cuhk.edu.cn

Abstract: With a high-resolution characterization setup, waveguide modes are clearly observed in near-field radiation patterns of SiNx nano-antennas. This phased array has uniform emission throughout the antenna within 3dB bandwidth of 120 nm from 785-905 nm. © 2023 The Author(s)

1. Introduction

The chip-scale optical phased arrays (OPAs) have found many applications of wireless optical communications and light detection and ranging (LiDAR) [1-3]. Silicon nitride (SiNx) nanophotonic phased arrays can work in wide wavelength range [4-7] and accommodate high on-chip optical power [8]. Beam steering on SiNx OPA has been demonstrated by phase modulated antennas [9], wavelength tuning [10, 11], and optimized cladding [12-14]. However, optical radiation properties within the whole OPA aperture have not been clearly investigated for SiNx nanophotonic phased arrays so far, which play critical roles of OPA outcoupling efficiency, beam steering angle, resolution, etc. In this work, we use a high-resolution imaging setup to characterize the near- and far-field radiation patterns on SiNx OPA and uniform emission is experimentally validated in wide wavelength range from 785 nm to 905 nm.

2. Device Structure and Characterization Setup

In Fig. 1(a), a 32-channel SiNx phased array is fabricated, and a 5-order cascaded 1×2 multimode interferometer (MMI) splitter tree is employed in the OPA to split the input laser into 32 waveguides with 550-nm width and 300-nm thickness. The MMI waveguide is 3.3-μm wide and 12-μm long with the input/output waveguide width of 1.1 μm and the gap of output waveguide of 1.1 μm. The antenna array pitch is 4.5 μm and the antenna is 146 μm long, as shown by scanning electron microscopy (SEM) images in Fig. 1(b)-(d). The grating periods and grating tooth width are modified to form a circle spot in the far-field projections as discussed in [15]. A high-resolution imaging system is constructed to characterize the near- and far-field radiation patterns of the OPA chip. In Fig. 1(e) of near-field imaging mode as demonstrated in [16-17], the chip is magnified by the lens set with the microscope objective, L1, L2, and L3, and finally imaged on a high-resolution CMOS camera. Then the system with resolution as high as 9000 × 5064 is achieved for imaging the radiation patterns outcoupled from OPA chips. Alternatively, in Fig. 1(f), the far-field radiation patterns in the Fourier space are directly imaged to the camera by objective, L1, and L3 with L2 lens removed. This setup can be used to observe the far field of the phased array directly on the back focal plane

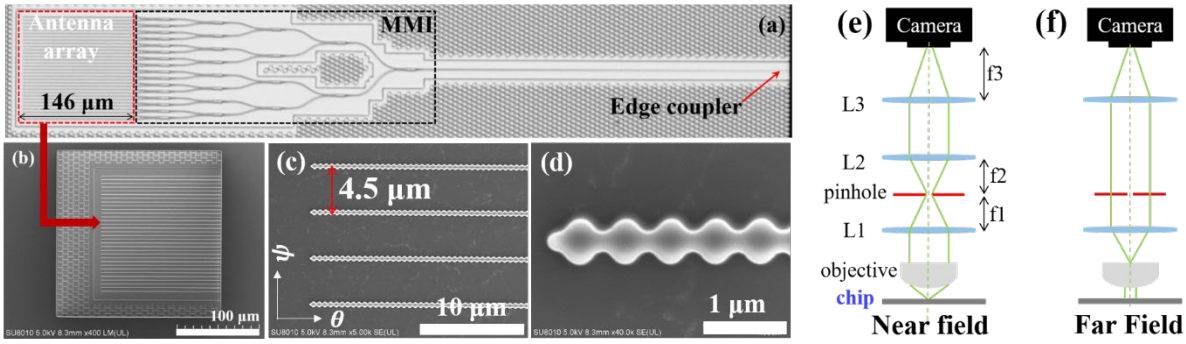

Fig. 1. (a) Image of the chip-scale OPA from an optical microscopy. Dashed red block shows the optical aperture with OPA antennas. (b)-(d) SEM images of the grating antenna array from the opening window with 32 antennas (b), 4 antennas (c) and 1 antenna (d), respectively. (e)-(f) The sketch of the high-resolution imaging setup, configured as a near-field imaging mode in the real space (e), and configured as a far-field imaging mode in the Fourier space (f).

of a high-numerical aperture (NA) microscope objective, wherein each coordinate (sinθ, sinψ) corresponds to a unique direction of OPA emission. An objective lens with a NA = 0.55 and angular radius of ~30° is used to observe the far-field patterns of the OPA chips to measure the wide-angle beam steering. A polarization controller is used to adjust the polarization of the laser coupled on the chip. Both TE and TM polarization can be transmitted by the OPA as mentioned in our previous work [4-7]. Only TE polarization is presented in the following results.

3. Experimental Results and Discussion

Fig. 2(a), Fig. 2(b) and Fig. 2(c) presents the near-field radiation images of a 146 μm × 146 μm phased array at different wavelengths of 785 nm, 850 nm, and 905 nm, respectively. We can find uniform emission throughout the

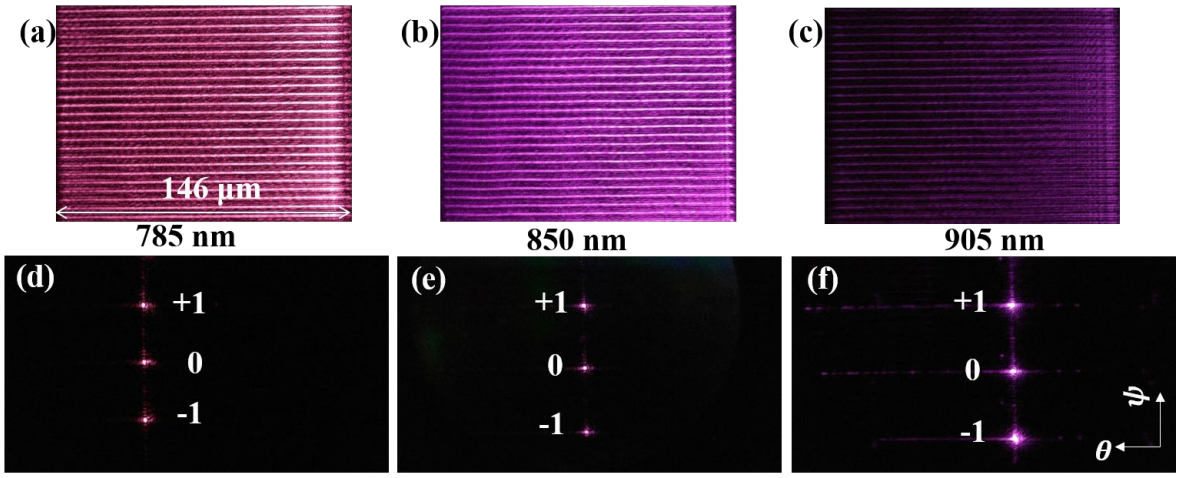

Fig. 2. Characterization results of OPA device. (a)-(c) High-resolution near-field patterns at different wavelengths of 785 nm, 850 nm, and 905 nm, respectively. (d)-(f) Far-field radiation patterns at different wavelengths of 785 nm, 850 nm, and 905 nm, respectively.

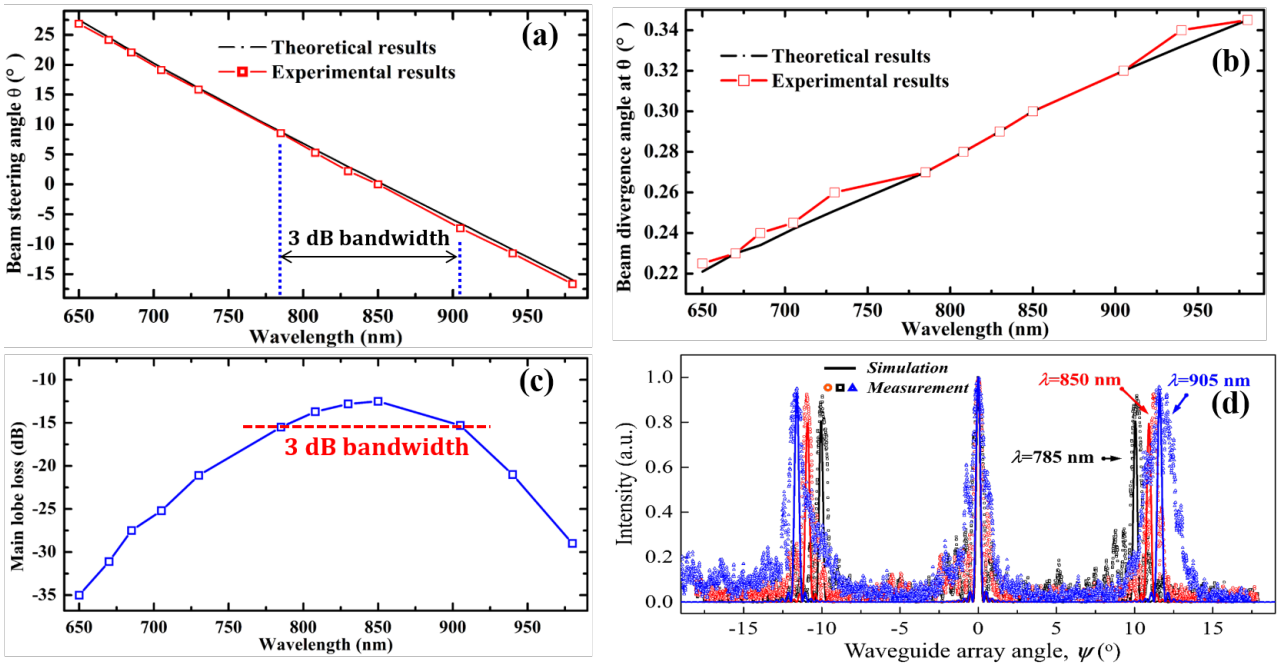

Fig. 3. The beam steering angles of main grating lobe (a) and the beam divergence angle (b) at different wavelengths in the θ direction. (c) The measured main-lobe loss versus different wavelengths. (f) Measured and theoretical ψ-direction profiles of Fig. 2(d)-(f).

146-μm long antennas for all these three wavelengths. And 32 waveguide modes propagating in antennas are clearly identified in high-resolution near-field radiation patterns (only 25 antennas are shown in each image since the chip size of CMOS camera is not large enough to capture all 32 antennas in the array direction, ψ). The corresponding far-field radiation patterns are shown in Fig. 2(d)-(f), with 0-order main lobe and +1-order/-1-order grating lobes captured, when wavelengths of 785 nm, 850 nm, and 905 nm are coupled on the chip.

The beam steering angle θ follows the grating diffraction equation, $sin\theta=n_{eff}-\lambda/\Lambda$, as mentioned in [4-5,7], and theoretical results are provided in Fig. 3(a). Experimental results for steering angle θ versus wavelength from 650 nm to 980 nm are also presented in Fig. 3(a). There is an obvious beam steering upon wavelength tuning in in the θ direction from +8.5° (at 785 nm) to -7.3° (at 905 nm). The beam divergence angles ψ_{FWHM} at θ depicted in Fig. 3(b) have good agreement with theoretical diffraction limit, $\psi_{FWHM}\approx0.886\lambda/Ndcos\psi$. The losses of the main-lobe beams are measured for 650-980 nm wavelengths and about 120 nm 3 dB bandwidth from 785 nm to 905 nm is marked in Fig. 3(c) and the corresponding beam steering angles are from +8.5° (at 785 nm) to -7.3° (at 905 nm) as shown in Fig. 3(a). The ψ-direction profiles of main lobe and grating lobes at wavelengths of 785 nm, 850 nm, and 905 nm, respectively, are shown in Fig. 3(d). The position of grating lobes can be calculated by the equation: $\psi'=\pm sin^{-1}(\lambda/d)$. The measured positions are well consistent with the theoretical calculations. The minor differences of <0.2° are mainly due to the measurement errors. And the beam divergence angles ψ_{FWHM} of the main lobes also match closely with theoretical predictions based on the previous diffraction equation $\psi_{FWHM}\approx0.886\lambda/Ndcos\psi$.

4. Conclusion

In conclusion, we have characterized the radiation properties of a 146 μm × 146 μm SiNx nanophotonic phased array, with the help of a high-resolution imaging setup for near- and far- field radiation patterns. It is validated that the OPA has the uniform emission throughout the whole antenna within its 3dB bandwidth of ~120 nm from 785 nm to 905 nm and demonstrates beam steering angles θ of +8.5° to -7.3° upon wavelength tuning from 785 nm to 905 nm. All 32 antennas in the OPA aperture are presented to radiate uniformly in high-resolution near-field radiation images.

5. Funding

National Natural Science Foundation of China (62175120); Guangdong Basic and Applied Basic Research Foundation (2021B1515120084); Tip-top Scientific and Technical Innovative Youth Talents of Guangdong Special Support Program (2019TQ05X062).

6. References

[1] C. V. Poulton, M. J. Byrd, P. Russo, E. Timurdogan, M. Khandaker, D. Vermeulen, and M. R. Watts, "Long-range LiDAR and free-space data communication with high-performance optical phased arrays," IEEE J. Sel. Top. Quantum Electron. 25(5), 1-8 (2019).
[2] X. Tang, R. Kumar, C. Sun, L. Zhang, Z. Chen, R. Jiang, H. Wang, and A. Zhang, "Towards underwater coherent optical wireless communications using a simplified detection scheme," Opt. Express 29(13), 19340-19351 (2021).
[3] Z. Chen, X. Tang, C. Sun, Z. Li, W. Shi, H. Wang, L. Zhang, A. Zhang, "Experimental demonstration of over 14 AL underwater wireless optical communication," IEEE Photon. Technol. Lett. 33(4), 173-176 (2021).
[4] C. Sun, L. Yang, B. Li, W. Shi, H. Wang, Z. Chen, X. Nie, S. Deng, N. Ding, and A. Zhang, "Parallel emitted silicon nitride nanophotonic phased arrays for two-dimensional beam steering," Opt. Lett. 46(22), 5699-5702 (2021).
[5] H. Wang, Z. Chen, C. Sun, S. Deng, X. Tang, L. Zhang, R. Jiang, W. Shi, Z. Chen, Z. Li, and A. Zhang, "Broadband silicon nitride nanophotonic phased arrays for wide-angle beam steering," Opt. Lett. 46(2), 286-289 (2021).
[6] H. Zhao, B. Kuyken, S. Clemmen, F. Leo, A. Subramanian, A. Dhakal, P. Helin, S. Severi, E. Brainis, G. Roelkens, and R. Baets, "Visible-to-near-infrared octave spanning supercontinuum generation in a silicon nitride waveguide," Opt. Lett. 40(10), 2177-2180 (2015).
[7] C. Sun, B. Li, W. Shi, J. Lin, N. Ding, H. Tsang, A. Zhang, "Large-Scale and Broadband Silicon Nitride Optical Phased Arrays," IEEE J. Sel. Top. Quantum Electron. 28(6), pp. 1-10, 2022.
[8] C. V. Poulton, M. J. Byrd, M. Raval, Z. Su, N. Li, E. Timurdogan, D. Coolbaugh, D. Vermeulen, and M. R. Watts, "Large-scale silicon nitride nanophotonic phased arrays at infrared and visible wavelengths," Opt. Lett. 42(1), 21-24 (2017).
[9] M. C. Shin, A. Mohanty, K. Watson, G. R. Bhatt, C. T. Phare, S. A. Miller, M. Zadka, B. S. Lee, X. Ji, I. Datta, and M. Lipson, "Chip-scale blue light phased array," Opt. Lett. 45(7), 1934-1937 (2020).
[10] Z. Chen, H. Wang, C. Sun, S. Deng, and A. Zhang, "Visible wavelength beam steering in silicon nitride nanophotonic phased arrays with a supercontinuum laser," Conf. Lasers Electro-Optics (CLEO), paper JW1A.22, 9-14 May 2021.
[11] C. Sun, B. Li, W. Shi, J. Lin, N. Ding, and A. Zhang, "Two-dimensional Visible and Near-infrared Beam Steering of Silicon Nitride Optical Phased Arrays," 2022 Conf. Lasers Electro-Optics (CLEO), paper JW3B.13, 15-20 May 2022.
[12] B. Li, C. Sun, H. Wang, Z. Chen, X. Nie, S. Deng, L. Yang, and A. Zhang, "Liquid-cladded optical phased array for a single-wavelength beam steering," Opt. Lett. 46(19), 4948-4951 (2021).
[13] B. Li, C. Sun, and A. Zhang, "Liquid Waveguide Cladding for 2D Beam Steering of an Optical Phased Array at a Single Wavelength," 2022 Optical Fiber Communications Conference and Exhibition (OFC), paper Th2A.3, 6-10 Mar. 2022.
[14] B. Li, C. Sun, and A. Zhang, "Optimization of the Far-field Pattern in an Apodized Optical Phased Array by Refractive Index Liquids," 2022 Conf. Lasers Electro-Optics (CLEO): Science and Innovations, paper JW3B.31, 15-20 May 2022.
[15] M. Raval, C. V. Poulton, and M. R. Watts, "Unidirectional waveguide grating antennas with uniform emission for optical phased arrays," Opt. Lett. 42(13), 2563-2566 (2017).
[16] X. Nie, C. M. Sun, H. Wang, Z. Chen, S. Deng, and A. Zhang, "Detection of near- and far-field radiation pattern of a silicon-on-insulator optical phase array," Conf. Lasers Electro-Optics (CLEO), paper JW1A.81 (2021).
[17] H. Wang, C. M. Sun, L. Yang, X. Nie, B. Li, and A. Zhang, "Uniform emission of large-scale optical phase arrays with wide wavelength tuning," 2021 Optical Fiber Communication Conference (OFC), paper W1D.5 (2021).